29th Congress of the International Council of the Aeronautical Sciences
St. Petersburg, Russia; September 7-12, 2014

ADAPTIVE FEEDFORWARD CONTROL DESIGN FOR GUST LOADS ALLEVIATION AND LCO SUPPRESSION

Wang, Y.*, Da Ronch, A., Ghandchi–Therani, M.**, Li, F.***
*China Academy of Aerospace Aerodynamics, Beijing, 100074, China
**University of Southampton, Southampton, S017 1BJ, United Kingdom

Keywords: *gust loads alleviation, LCO suppression, adaptive feedforward control, aeroelastic model.*

Abstract

An adaptive feedforward controller is designed for gust loads alleviation and limit cycle oscillations suppression. Two sets of basis functions, based on the finite impulse response and modified finite impulse response approaches, are investigated to design the controller for gust loads alleviation. Limit cycle oscillations suppression is shown by using the modified finite impulse response controller. Worst case gust search is performed by using a nonlinear technique of model reduction to speed up the costs of calculations. Both the "one–minus–cosine" and Von Kármán continuous turbulence gusts of different intensities were generated to examine the performance of controllers. The responses of these two types of gust can be reduced effectively by finite impulse response controller in the whole process, while the modified finite impulse response controller is found to increase the loads during the initial transient response. The above two types of gust induced limit cycle oscillations were used to test the modified finite impulse response controller. Results show that it can suppress limit cycle oscillations to some extent.

1 Introduction

To reduce the impact of air transport on the environment and improve aircraft global efficiency, a lightweight solution with high aspect ratio wings is usually needed [1]. For such aircraft, the frequencies of rigid body motions and aeroelastic vibrations have the tendency to get closer to each other, which increases the nonlinear aeroelastic coupling between flight mechanics and structural dynamics. Thus, atmospheric turbulence gusts significantly excite structural vibrations. These vibrations cause dynamic structural loads and influence the rigid body motions of the aircraft, which decreases handling qualities and passenger comfort. In practical conditions, gusts can induce limit cycle oscillations (LCOs), which are non-diverging, self-sustained, fixed-frequency structural vibration phenomena, and can cause fatigue issues and reduce the aircraft operational life.

Aeroelastic active control has been investigated for several decades, especially for flutter suppression and gust loads alleviation [2, 3, 4, 5]. Feedback control strategies, e.g. linear quadratic regulator (LQR), optimal control algorithm, H_∞ robust control synthesis, are relatively mature and have been used extensively in aeroservoelasticity for gust loads alleviation. When prior knowledge of disturbance is available, a feedforward control strategy is generally preferred over feedback control for disturbance rejection. One of the advantages of feedforward control is that there is no time delay between the disturbance and control compensation, which means that corrective action can be taken before the output has deviated from the set point. It is possible to design a feedforward controller to alleviate gust load response by measuring the vertical gust speed ahead of aircraft using light detection and ranging (LIDAR) beam airborne wind sensor [6]. Reference [7] developed a linear adaptive feedforward controller using orthonormal basis function for gust loads alleviation on linear aeroelastic model and good

performances were found.

The aim of this paper is to design an appropriate feedforward controller to control the response of an aerofoil system, including gust loads alleviation and LCOs suppression. The feedforward controller can be realized by two different basis functions, finite impulse response (FIR) model and modified finite impulse response (MFIR) model. Section 2 introduces the two degrees of freedom (DoF) aerofoil aeroelastic system used in this paper. The adaptive feedforward control design is formulated in Sec. 3. The turbulence gust models are reviewed in Sec. 4. An efficient worst–case–gust search for the "one–minus–cosine" family is presented in Sec. 5 using a nonlinear reduced order model [5]. Results for cases with strong nonlinear effects are shown in Sec. 6. Finally, conclusions are given.

2 Aeroelastic model

The aeroelastic model used in this paper, shown in Fig. 1, is a typical aerofoil section with two degrees of freedom that define the motion about a reference elastic axis (*e.a.*). The plunge deflection is denoted by h, positive downward, and α is the angle of attack about the elastic axis, positive with nose up. The semi–chord length is b. The nondimensional distances from the midchord to the elastic axis and from the elastic axis to the centre of gravity are a_h and x_α, respectively. The aerofoil is equipped with a massless trailing–edge flap with hinge at a distance cb from the midchord. The flap deflection, δ, is defined relative to the aerofoil chord. The motion is restrained by two springs, K_ξ and K_α, and the model is assumed to have a horizontal equilibrium position at $h = \alpha = \delta = 0$. The system contains structural damping in both degrees of freedom, C_ξ and C_α. The equations in dimension form with a polynomial nonlinearity for the restoring forces are

$$m\ddot{h} + S_\alpha\ddot{\alpha} + C_\xi\dot{h} + K_\xi(h + \beta_{\xi_3}h^3 + \beta_{\xi_5}h^5) = -L \quad (1)$$

$$S_\alpha\ddot{h} + I_\alpha\ddot{\alpha} + C_\alpha\dot{\alpha} + K_\alpha(\alpha + \beta_{\alpha_3}\alpha^3 + \beta_{\alpha_5}\alpha^5) = M \quad (2)$$

where m, S_α, and I_α are the aerofoil sectional mass, the first and second moment of inertia of aerofoil about elastic axis. The lift, L, is defined positive upward according to the usual sign convention in aerodynamics. The moment around the elastic axis is M. The plunge displacement, h, is positive downward, as it is conventionally done in aeroelasticity. The unsteady aerodynamics is modeled with strip theory and the incompressible two-dimensional classical theory of Theodorsen. The model [1] is formulated in first order and contains 12 states. More details can be found in Ref. [8].

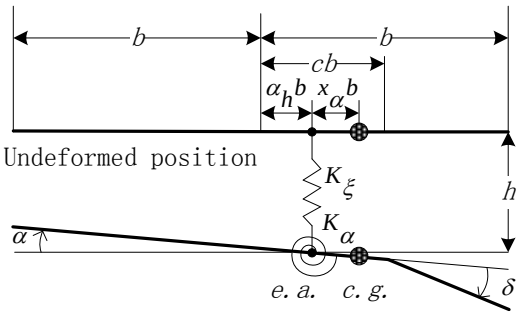

Fig. 1 : Schematic of an aerofoil section with trailing–edge flap; the wind velocity is to the right and horizontal; *e.a.* and *c.g.* denote, respectively, the elastic axis and centre of gravity

3 Feedforward control

A feedforward control system consists two channels, see Fig. 2. One channel is the disturbance transfer path and the other one is the control path. Denote w_g the atmospheric gust disturbance, and by $\hat{w}_g$ the gust measured by the on–board LIDAR sensor. In this paper, it is assumed that the measured gust, $\hat{w}_g$, is identical to the true atmospheric gust, w_g. The transfer function of the physical plant (in this case, the aerofoil section) between the gust disturbance and the structural response is denoted by H; G indicates the transfer function of the physical plant between the control effector (in this case, the trailing edge flap) and the structural response, and $\hat{G}$ indicates the approximate transfer function of $-G$. The feedforward controller

[1] The code can be obtained from Da Ronch, A., A.DaRonch@soton.ac.uk

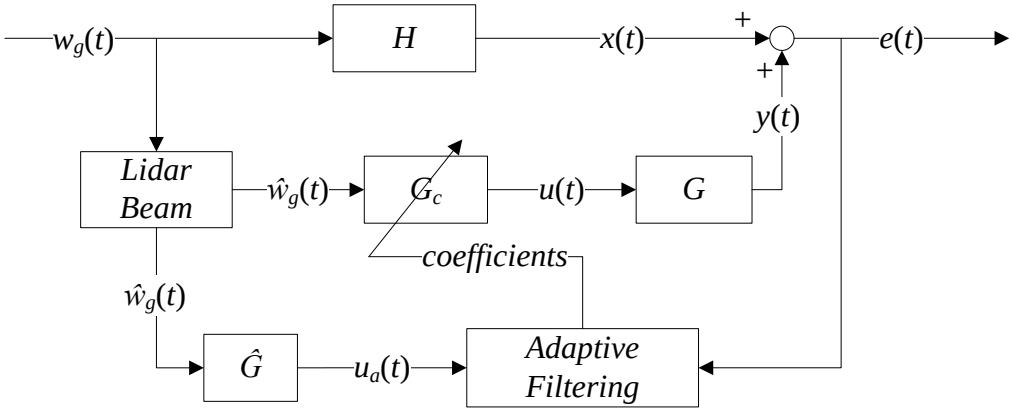

Fig. 2 : Block diagram of the adaptive feedforward control applied to a physical plant with transfer function H

is represented by G_c, and $u(t)$ indicates the controller output, e.g. the rotation of the trailing edge flap.

The object of this study is to design the feedforward controller G_c to control the gust response of the nonlinear aerofoil model. Theoretically, the ideal feedforward controller G_{c_i} is

$$G_{c_i} = -HG^{-1} \tag{3}$$

The method used to evaluate the controller model (transfer function) is based on a prediction error minimization (PEM) approach.

First, PEM is used to identify $\hat{G}$, an approximation model of the control path G

$$\hat{G} \approx -G \tag{4}$$

which is done by performing an experiment, e.g. using an external signal $u(t)$ to inject into the flap as the excitation signal, and the response signal $y(t)$ as the output signal. Then, using $\hat{G}$ to filter the measured gust signal $\hat{w}_g(t)$ and then get an output response $u_a(t)$, which is

$$u_a(t) = \hat{G}w_g(t) \tag{5}$$

Here it is assumed that $\hat{w}_g(t)$ is equal to $w_g(t)$. In the disturbance path, the relationship of response $x(t)$ and gust $w_g(t)$ is

$$x(t) = Hw_g(t) \tag{6}$$

Substituting (5) into (6) yields to

$$x(t) \approx -HG^{-1}u_a(t) \tag{7}$$

Finally, the information about the physical system for feedforward control can be identified by using $u_a(t)$ as input and $x(t)$ as output. Adaptive strategy is used to ensure the robustness of the feedforward controller. The coefficients of the controller are computed by an adaptive filtering algorithm. In practice, $x(t)$ is replaced by $e(t)$, which is the error between the disturbance response and the control path response measured by a sensor.

The controller is considered as a discrete linear time invariant system

$$u(t) = G_c(q)\hat{w}_g(t) \tag{8}$$

where $\hat{w}_g(t)$ is the input signal and $u(t)$ is the corresponding output signal. $G_c(q)$ is transfer operator represented the controller, where q is the forward shift operator, $q\hat{w}_g(t) = \hat{w}_g(t+1)$, and q^{-1} is the delay (backward shift) operator, $q^{-1}\hat{w}_g(t) = \hat{w}_g(t-1)$. The corresponding transfer function $G_c(z)$, $z \in C$ (the complex plane), which is formulated as

$$G_c(z) = \sum_{k=1}^{n} L_k B_k(z) \tag{9}$$

where $B_k(z)$ are basis functions, L_k are the corresponding coefficients, and n is the model order. In this paper two kinds of basis functions based on FIR model and MFIR model were used to approximate the ideal feedforward controller. These two methods are discussed in the following section.

3.1 Finite Impulse Response model

A FIR model of Eq. (9) corresponds to the choice

$$B_k(z) = z^{-k}, k = 1,2,\cdots,n \qquad (10)$$

where n is the order of model chosen by the balance of the approximation accuracy and computational cost. The FIR model structure is shown in Fig. 3. So the FIR model means using a number of transfer functions with zero poles to approximate the controller.

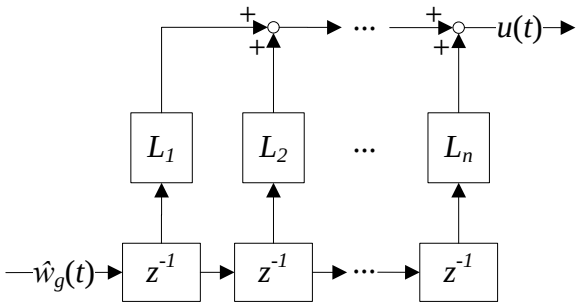

Fig. 3 : Structure of FIR model

3.2 Modified Finite Impulse Response model

If the real system dynamics have a slow pole, then the model order n will be very large to provide an accurate approximation to the true dynamics. One strategy to overcome this is to instead choose

$$B_k(z) = \prod_{k=1}^{n} \frac{1}{z-\xi_i}$$
$$k = 1,2,\cdots,n; i = 1,2,\cdots,k \qquad (11)$$

where $\{\xi_i\}_{i=1,2,\ldots,n}$ is a set of chosen poles [9], which means injecting *a priori* knowledge into basis functions. The MFIR model structure is shown in Fig 4. For the treatment of multiple complex poles, see Ref. [9] for guidelines.

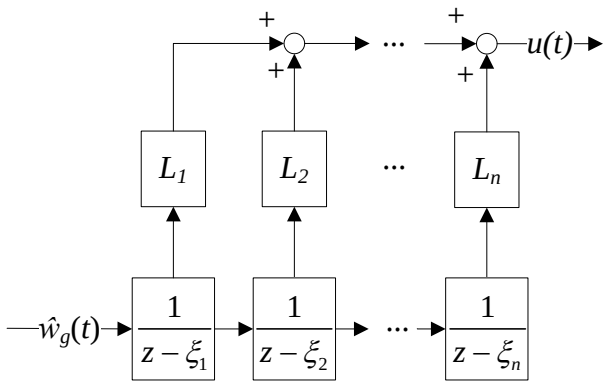

Fig. 4 : Structure of MFIR model

3.3 Exponentially weighted recursive least-square algorithm

The coefficients of the basis functions are calculated by exponentially weighted recursive least-square algorithm. Donate a cost function by

$$\varepsilon(N) = \sum_{i=1}^{N} \lambda^{N-i} |\hat{e}(i)|^2$$
$$0 < \lambda \leq 1, N = 1,2,\cdots \qquad (12)$$

where N is the total number of time steps, λ is the forgetting factor, and $\hat{e}(i)$ is the error between the desired response $e(i)$ and the FIR or MFIR model output $z(i)$ at time i

$$\hat{e}(i) = e(i) - z(i) = \hat{e}(i) - L(N)\Phi^T(i) \qquad (13)$$

the vector $\Phi^T(i) = [u_{a_1}(i), u_{a_2}(i), \cdots, u_{a_n}(i)]^T$ is the output of every basis function of the FIR or MFIR model, and $L(i) = [L_1(i), L_2(i), \cdots, L_n(i)]$ is the corresponding coefficient vector, or called tap weight vector. The adaptive algorithm includes the following steps:

- Initialize

  $L(0) = 0,$

  $P(0) = \delta^{-1} I$, where δ is a small positive constant (e.g. 1.0).

- Iterate for each instant of time, $N = 1,2,\cdots$, compute

$$\pi(N) = P(N-1)\Phi(N) \tag{14}$$

$$k(N) = \frac{\pi(N)}{\lambda + \Phi^T(N)\pi(N)} \tag{15}$$

$$\varepsilon(N) = d(N) - L^T(N-1)\Phi(N) \tag{16}$$

$$L(N) = L(N-1) + k(N)\bar{\varepsilon}(N) \tag{17}$$

$$P(N) = \lambda^{-1}P(N-1) - \lambda^{-1}k(N)\Phi^T(N)P(N-1) \tag{18}$$

where $P(N)$ is the inverse correlation matrix, $k(N)$ is a gain vector, and $\pi(N)$ is a middle variable which is used to increase the computation accuracy. The forgetting factor λ should be carefully chosen. By default, the value 1.0 is used. More details about this algorithm can be found in Ref. [10].

4 Turbulence gust model

For aircraft certification, gust loads are critical for structural sizing. Two types of atmospheric gust model were used in this paper. The discrete model based on the "one–minus–cosine" shape is formulated as

$$w_g(t) = \frac{w_0}{2}\cos\left(\frac{2\pi}{H_g}\frac{U}{b}(t-t_0)\right) \qquad t_0 \le t \le t_0 + \frac{H_g b}{U} \tag{19}$$

where w_0 is the gust intensity normalized by the freestream speed U, H_g is gust wave length normalized by aerofoil semi–chord. The physical time is t. The Von Kármán spectrum is used for the continuous model. According to MIL-F-8785C, the vertical spectrum function is

$$\phi_w(\omega) = \frac{\sigma_w^2 L_w}{\pi U}\cdot\frac{1+\frac{8}{3}\left(1.339L_w\frac{\omega}{U}\right)^2}{\left[1+\left(1.339L_w\frac{\omega}{U}\right)^2\right]^{11/6}} \tag{20}$$

where $\phi_w(\omega)$ is the energy spectral density, σ_w is the turbulence intensity, ω is the circular frequency, and L_w represents the turbulence scale length. The turbulence is generated by passing a band–limited white noise through an appropriate forming filter with transfer function

$$H_w(s) = \frac{\sigma_w\sqrt{\frac{1}{\pi}\cdot\frac{L_w}{U}}(1+A(s))}{1+B(s)}$$

$$A(s) = 2.7478\frac{L_w}{U}s + 0.3398\left(\frac{L_w}{U}\right)^2 s^2$$

$$B(s) = 2.9958\frac{L_w}{U}s + 1.9754\left(\frac{L_w}{U}\right)^2 s^2 + 0.1539\left(\frac{L_w}{U}\right)^3 s^3 \tag{21}$$

The turbulence intensity is

$$\sigma_w = 0.1 w_{20} \tag{22}$$

where w_{20} is the wind speed at 20 feet (6 m). Typical value for light turbulence, the wind speed at 20 feet is 15 knots; for moderate turbulence, the wind speed is 30 knots; and for severe turbulence, the wind speed is 45 knots.

5 Worst–case–gust search

Regarding to an aircraft system, when the frequency of gust is close to a frequency of one mode, the response would become larger, which is the worst case gust corresponding to this mode. In this paper, the worst–case–gust search for "one–minus–cosine" family was performed. To reduce computational cost, reduced–order model (ROM) combined with kriging interpolation technique was used to perform the worst–case–gust search. The detailed derivation of ROM can be found in Ref. [1]. Assuming the pitch and plunge frequencies of the aerofoil system are f_α and f_ξ, respectively, the wave lengths of the worst case gust corresponding to these two modes are

$$H_{g_\alpha} = \frac{U}{f_\alpha b}, H_{g_\xi} = \frac{U}{f_\xi b} \tag{23}$$

which can be represented in nondimensional form

$$H_{g_\alpha} = \frac{2\pi U}{\omega_\alpha b} = 2\pi U^*, H_{g_\xi} = \frac{2\pi U}{\omega_\xi b} = \frac{2\pi U^*}{\bar{\omega}} \tag{24}$$

where ω_α is the pitch mode circular frequency and ω_ξ is the plunge mode circular frequency, $\bar{\omega}$

is the ratio between ω_ξ and ω_α. U^* is reduced velocity, equal to $U/b\omega_\alpha$. Equation (24) shows that the worst case gust wave length for pitch and plunge are influenced by freesteam velocity and corresponding circular frequency.

6 Results

In this work, results are presented for a nonlinear aeroelastic model of a pitch–plunge aerofoil. The model is representative of a wind tunnel test rig installed at University of Liverpool. The aeroelastic parameters are summarized in Table 1 (see, e.g. Ref. [1] for their definitions). The air mass ratio is represented by μ, ζ_α and ζ_ξ are the viscous dampings of plunge and pitch, and r_α is nondimensional radius of gyration about the elastic axis. The values of β_{ξ_3} and β_{ξ_5} for the linear system are 0. The wind tunnel aeroelastic model has the following parameters which were measured at the University of Liverpool: wing semichord $b = 0.175$ m, pitch circular frequency $\omega_\alpha = 28.061$ rad/s, plunge circular frequency $\omega_\xi = 16.629$ rad/s.

Table 1: Aeroelastic parameters

Parameter	Value
$\bar{\omega}$	0.593
μ	69.000
a_h	-0.333
x_α	0.090
r_α	0.400
ζ_α	0.015
ζ_ξ	0.015
β_{ξ_3}	1741.881
β_{ξ_5}	638721.901

6.1 Validation results

The predictions of the coupled aeroelastic model are compared to data measured from the aeroelastic model in the low–speed, open–loop wind tunnel of the University of Liverpool. Figure 5 shows the numerical and the wind tunnel experimental results of damped natural frequency and damping ratios for varying freestream speeds. The predictions for the pitch mode agree well with the measured data. Some difference are noticed for the plunge mode. More comparisons between aeroelastic model and experiment can be found in [8].

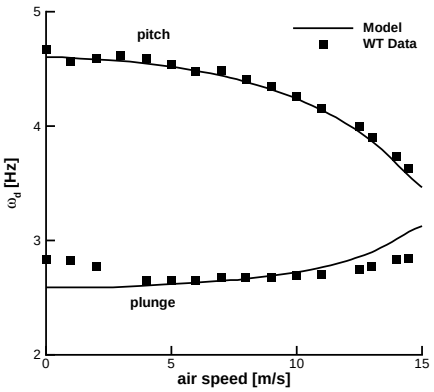

(a) Damped frequency

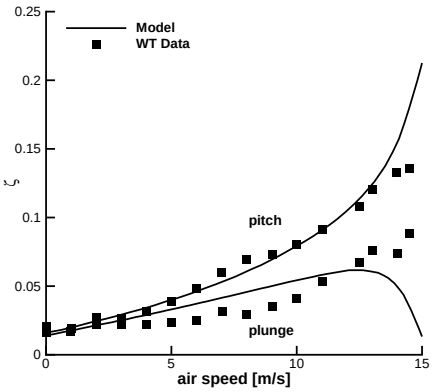

(b) Damping ratio

Fig. 5 : Eigenvalues tracing for varying freestream speed from simulation and wind tunnel measurements of the aerofoil test rig

The nonlinear aeroelastic model exhibits interesting dynamics below the flutter speed of 15.28 m/s, and this is shown in Fig. 6. Whereas at the lower speed of 8 m/s the aerofoil response is well damped , a LCO arises at 13 m/s.

6.2 Worst–case–gust search

Identification of the worst case gust allows identifying for critical gust loads used to verify the effectiveness of the control approaches. The approach to model reduction [1, 5, 8, 11] was used

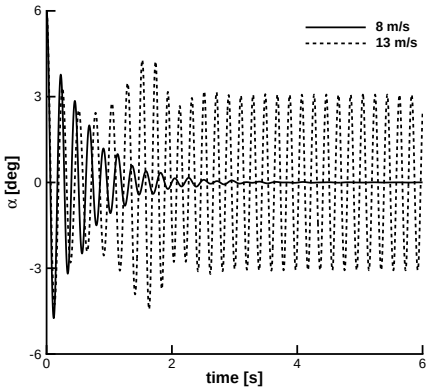

(a) Pitch

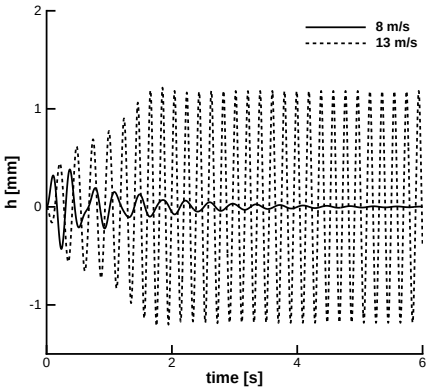

(b) Plunge

Fig. 6 : Open loop/ uncontrolled responses for an initial angle of attack of 6 deg at speeds of 8 and 13 m/s

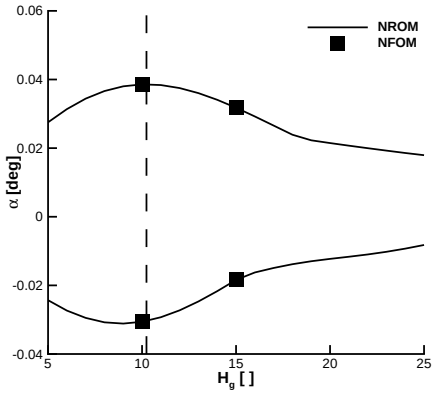

(a) Pitch

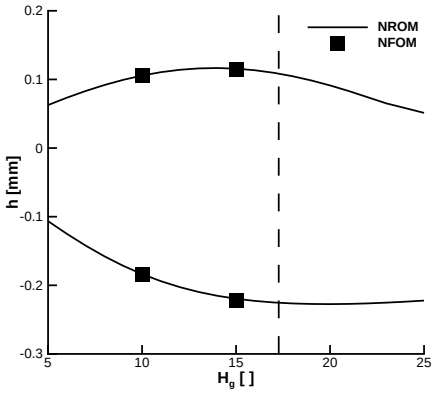

(b) Plunge

Fig. 7 : Worst–case–gust search for the "one–minus–cosine" gust of intensity 0.005 at freestream speed of 8 m/s; the vertical line denotes the gust wavelength calculated from Eq. 24

to generate a reduced model, which allows retaining the nonlinear dynamics exhibited by the original coupled aeroelastic model, is smaller in size and computationally more efficient. For model projection, 3 modes were used (see Ref. [1]). This model was used in combination with the Kriging approach to predict the worst–case–gust profile.

6.2.1 Light "one–minus–cosine" gust

An intensity of 0.005 "one–minus–cosine" gust was investigated first, and results are shown in Fig. 7. The solid curves in the top plot are nonlinear ROM (NROM) results, while the solid squares are computed by nonlinear full–order model (NFOM). The figures show that the NROM and NFOM results agree well. The worst case gust wavelengths for pitch and plunge at intensity of 0.005 are 10 and 16 semi–chords. When freestream speed is 8 m/s, U^* is 1.629 and $\bar{\omega}$ is 0.593, H_{g_α} and H_{g_ξ} calculated by Eq. 24 are 10.235 and 17.260 semi–chords, which are shown in Fig. 7 as dashed lines. The worst case gust corresponding to pitch mode has a good agreement between search result and the value calculated by Eq. 24, while there is a small difference for the plunge mode.

6.2.2 Strong "one–minus–cosine" gust

For a strong gust intensity of 0.1, the structural nonlinearities influence the prediction of

the worst–case–gust wavelength compared to the linear case, which are shown in Fig. 8. The

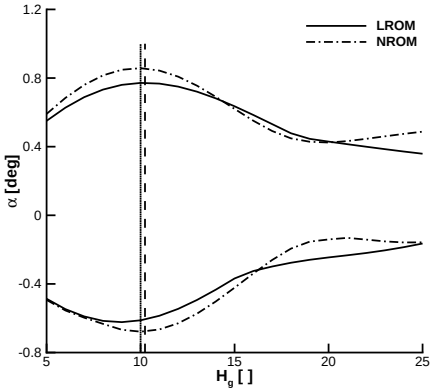

(a) Pitch

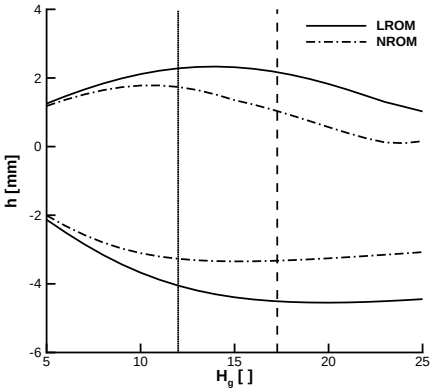

(b) Plunge

Fig. 8 : Worst–case–gust search for the "one–minus–cosine" gust of intensity 0.1 at freestream speed of 8 m/s; the vertical dashed and dotted line denote the worst case gust wavelength of linear and nonlinear system, respectively

solid curves are the linear system results by using linear reduced–order model (LROM), while the dashed dot curves are corresponding to the nonlinear system using NROM. The worst case gust wavelengths of the linear system for pitch and plunge at intensity of 0.1 are the same as the case of light intensity of 0.005. In terms of the nonlinear system, the worst case gust wavelength of pitch at this intensity is still 10 semi–chords, while the worst case gust of plunge is 12, which is different from the linear system and the value computed by Eq. (24). It is because of the nonlinear hardening effect when encountering strong gust. This effect reduces the gap between pitch and plunge vibration frequencies. Nonlinearities also deteriorate the worst case gust for pitch mode which increase its amplitude.

6.3 Gust loads alleviation

Gust loads alleviation to both discrete "one–minus–cosine" and continuous Von Kármán atmospheric turbulence will be performed by using FIR and MFIR controllers. Corresponding to each type of gust, light and strong intensities will be investigated. The freestream speed used in this section is low speed of 8 m/s, a higher speed of 13 m/s will be considered in Sec. 6.4.

6.3.1 Light Atmospheric Turbulence

The nonlinear open loop and control responses to multiple cycles of "one–minus–cosine" gust for pitch and plunge at intensity of 0.005 and wavelength of 10 semi–chords (worst case for pitch mode) by using FIR and MFIR controllers are shown in Fig. 9. Both FIR and MFIR controllers exhibit the ability to alleviate gust loads response for pitch. Nearly half of the pitch amplitude is reduced by the FIR and MFIR controllers from around 0.15 deg to 0.08 deg at steady stage. Aircraft will benefit from this gust loads alleviation effects, e.g. fatigue resistance and improving passenger comfort. The FIR control response takes a long time to converge to a constant amplitude, while the MFIR controller shows a fast convergence in 5 seconds. The reason is that MFIR controller considers the poles of the system in the basis functions, see Sec. 3.2.

The controllers designed in the paper aim to alleviate the pitch response. The plunge control response is here verified, see Fig. 9. The plunge response amplitudes of the two controllers are close to the open loop at steady stage, while the mean values increase some. There are some peak values for pitch and plunge by using the MFIR controller at the initial period, which are bigger than the open loop responses , while the control responses by using FIR controller are stable and changing gradually in the whole control process.

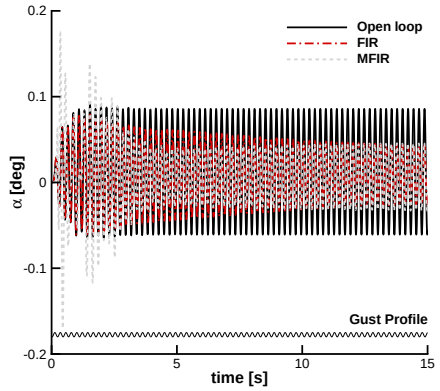

(a) Pitch

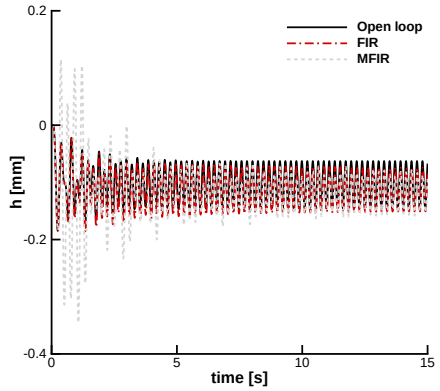

(b) Plunge

Fig. 9 : Open loop and control responses to a multi–cycle "one–minus–cosine" gust with intensity of 0.005 and wavelength of 10 semi–chords at freestream speed of 8 m/s

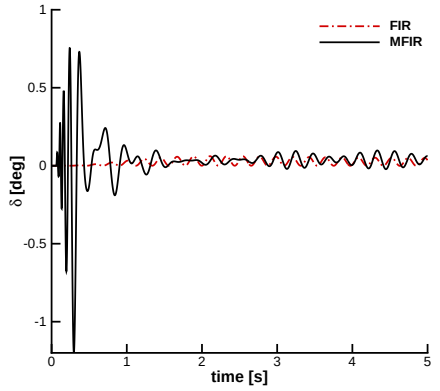

Fig. 10 : Flap rotation to a multi–cycle "one–minus–cosine" gust with intensity of 0.005 and wavelength of 10 semi–chords at freestream speed of 8 m/s

The initial five seconds output of the FIR and MFIR controllers, which are the rotation input of the flap in this case, are shown in Fig. 10.

The flap rotation of the MFIR controller is very large at the beginning, while the values of the FIR controller are close to zero. At steady stage, the flap rotation of the MFIR controller become smaller but it is still bigger than the FIR controller. All the flap rotation and corresponding velocity of the two controllers are smaller than the practical experimental limits: -7 deg $\leq \delta \leq$ 7 deg, $\dot{\delta} \leq$ 15 Hz.

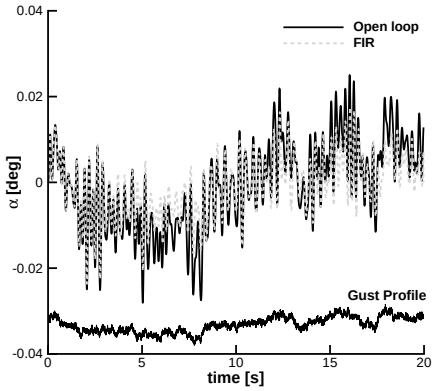

(a) Pitch

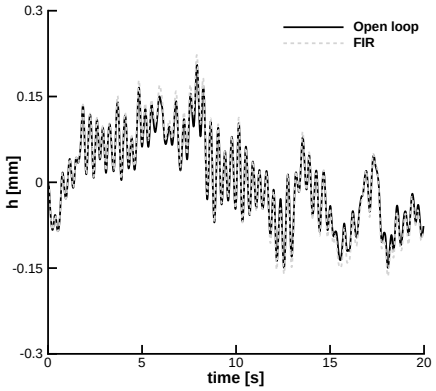

(b) Plunge

Fig. 11 : Open loop and control responses to a Von Kármán gust (h = 10,000 m, intensity = 10^{-2}, 'light') with peak amplitude intensity of 0.005 at freestream speed of 8 m/s

The Von Kármán turbulence model was used to generate the continuous gust. Light turbulence gust was computed at 10,000 meters height

and freestream speed of 8 m/s with light intensity of 10^{-2}. The peak amplitude of gust intensity is 0.005, which is the same as the light "one–minus–cosine" gust. The open loop and control responses to this gust using FIR controller are shown in Fig. 11. Like in "one–minus–cosine" gust control, the MFIR controller exhibits even worse control characteristics at the beginning stage which is not shown here. The FIR controller has effect control on light Von Kármán continuous gust for pitch, while small difference is found for plunge between open loop and control responses. The FIR controller reduces the amplitude and mean value of the pitch response, which will decrease the gust impact on aircraft fatigue and extend the operation life. The flap rotation of the FIR controller shown in Fig. 12 and corresponding velocity are within the experimental setting limits.

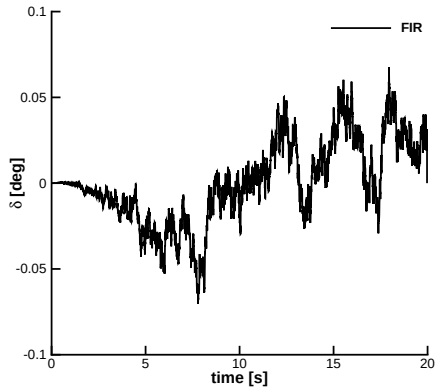

Fig. 12 : Flap rotation to a Von Kármán gust (h = 10,000 m, intensity = 10^{-2}, 'light') with peak amplitude intensity of 0.005 at freestream speed of 8 m/s

6.3.2 *Strong Atmospheric Turbulence*

A stronger gust intensity is here investigated to verify the control approach in cases where the structure nonlinearity is strongly affects the system responses.

The open loop and control responses to "one–minus–cosine" gust with intensity of 0.1 and wavelength of 10 semi–chords (worst case for pitch mode) are shown in Fig. 13. Compared with light intensity of "one–minus–cosine" gust, the FIR controller shows better performance for strong "one–minus–cosine" gust, which converged to stable state quickly. The beginning stage of MFIR control is still not good. Both controllers show effective gust loads alleviation functions for pitch. The amplitude of pitch was reduced from around 3.9 deg to 2.1 deg. The mean values of plunge response by using the two controllers was increased from around -1.5 mm to -1.8 mm. The flap rotation is shown in Fig. 14. The initial flap rotation of the MFIR controller even gets to the setting limits.

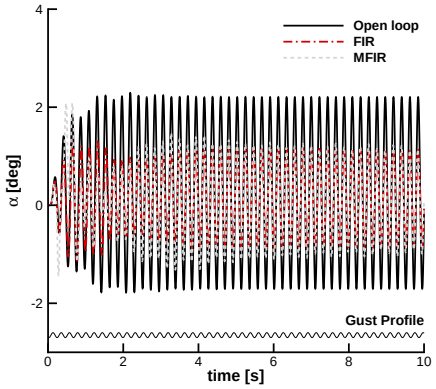

(a) Pitch

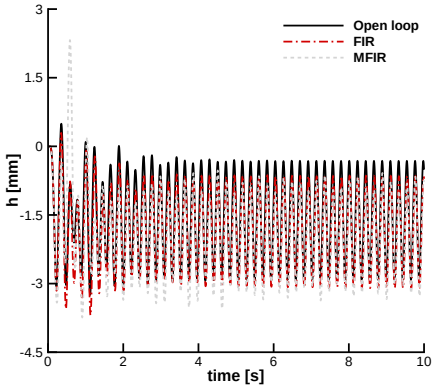

(b) Plunge

Fig. 13 : Open loop and control responses to a multi–cycle "one–minus–cosine" gust with intensity of 0.1 and wavelength of 10 semi–chords at freestream speed of 8 m/s

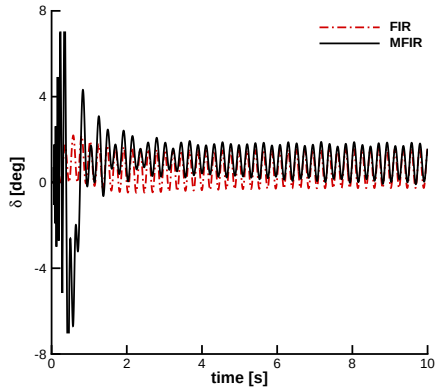

Fig. 14 : Flap rotation to a multi–cycle "one–minus–cosine" gust with intensity of 0.1 and wavelength of 10 semi–chords at freestream speed of 8 m/s

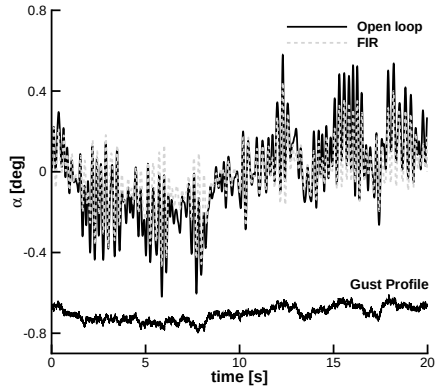

(a) Pitch

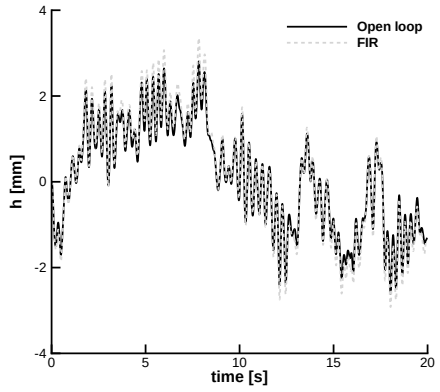

(b) Plunge

Fig. 15 : Open loop and control responses to a Von Kármán gust (h = 10,000 m, intensity = 10^{-5}, 'severe') with peak intensity of 0.1 at freestream speed of 8 m/s

Figure 15 shows the open loop and control responses to Von Kármán turbulence gust by using FIR controller. The gust was generated by Von Kármán turbulence model at altitude of 10,000 meters and freestream speed of 8 m/s with severe intensity of 10^{-5}. The peak amplitude of gust intensity is 0.1. The control responses of pitch and plunge show similar characteristics to the results of light Von Kármán turbulence gust. The flap rotation of FIR controller is shown in Fig. 16. All the values are located in the setting range.

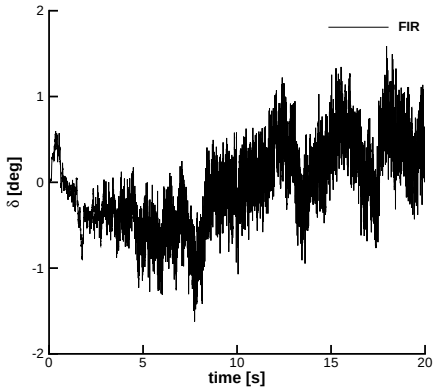

Fig. 16 : Flap rotation to a Von Kármán gust (h = 10,000 m, intensity = 10^{-5}, 'severe') with peak intensity of 0.1 at freestream speed of 8 m/s

6.4 Limit Cycle Oscillations suppression

It was observed that the nonlinear system exhibits LCOs below the flutter speed above a speed of 12.45 m/s. In this section, the suppression of a gust–induced LCO response is investigated at a freestream speed of 13 m/s (85% of the flutter speed). A comparison between prediction and measured LCOs is reported in Ref. [12].

6.4.1 "One–minus–cosine" gust induced LCO

Figure 17 shows the open loop and control responses by using FIR and MFIR controllers in terms of a one–cycle "one–minus–cosine" gust induced LCO at 13 m/s. It is suggested that the MFIR controller has good effect to suppress LCO for both degrees of freedom, which reduces the pitch amplitude from 6 deg to 4 deg and plunge

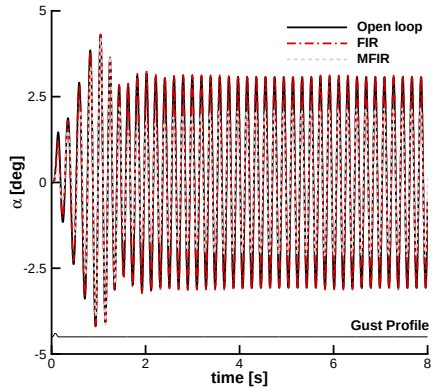

(a) Pitch

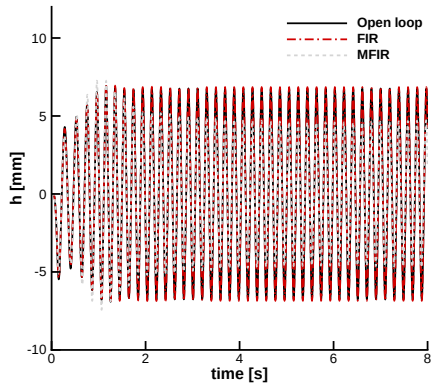

(b) Plunge

Fig. 17 : Open loop and control responses to a one–cycle "one–minus–cosine" gust with peak intensity of 0.1 at freestream speed of 13 m/s

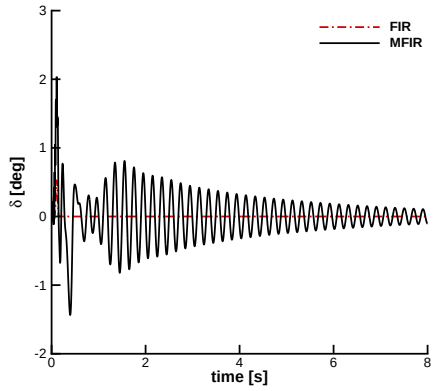

Fig. 18 : Flap rotation to a one–cycle "one–minus–cosine" gust induced LCO suppression at freestream speed of 13 m/s

amplitude from 14 mm to 9 mm. The FIR controller doesn't have reduction effect for the pitch and plunge responses. The reason can be found from the output signal of controller shown in Fig. 18, which is the input of flap. The output of the FIR controller converges to zero quickly, while the output of the MFIR controller attenuates slowly, which means that there is still effective input for the flap to suppress LCO after switching off the gust input.

6.4.2 Von Kármán turbulence induced LCO

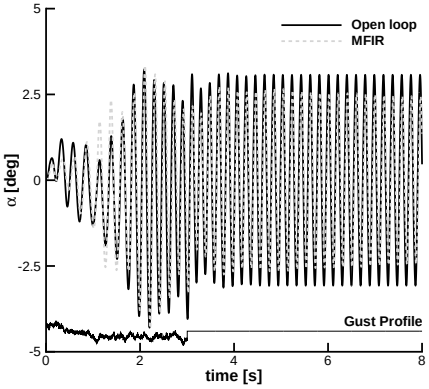

(a) Pitch

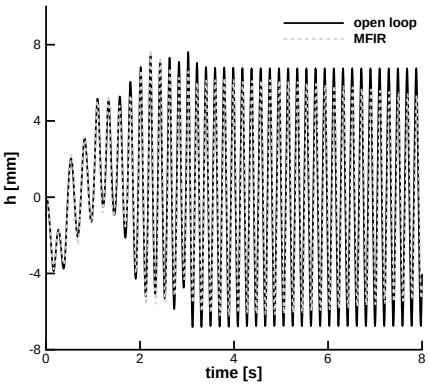

(b) Plunge

Fig. 19 : Open loop and control responses to a Von Kármán turbulence gust induced LCO suppression at freestream speed of 13 m/s

A Von Kármán turbulence induced LCO and control response by using MFIR controller are shown in Fig. 19. The Von Kármán turbulence

last for 3 seconds from the beginning. The amplitude of pitch and plunge responses were reduced from 6 deg to 5 deg and from 14 mm to 11 mm. Here the control results by using FIR controller is omitted, which doesn't have any LCO suppression effect. The flap rotation input of the MFIR controller shown in Fig. 20 meet the limit requirements.

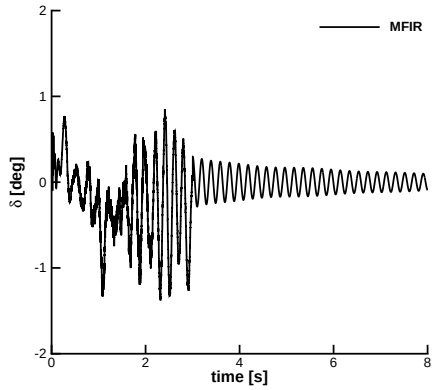

Fig. 20 : Flap rotation and velocity to a Von Kármán turbulence gust induced LCO suppression at freestream speed of 13 m/s

7 Conclusions

This paper investigated adaptive feedforward control for gust loads alleviation and limit cycle oscillations (LCOs) suppression. Two kinds of basis functions, finite impulse response (FIR) and modified finite impulse response (MFIR), were used to design the controller. The robustness was increased by using an adaptive control strategy. The test case is a nonlinear aeroelastic aerofoil section, with pitch and plunge as degrees of freedom. The following considerations can be drawn from the present work:

- The FIR controller shows good control effect for multi–cycle "one–minus–cosine" and Von Kármán turbulence gust loads alleviation, while the MFIR controller tends to increase the amplitude during the initial transient of the response.
- The MFIR controller was found adequate to reduce the amplitude of the "one–minus–cosine" and Von Kármán turbulence gust–induced limit cycle oscillations for both pitch and plunge degrees of freedom.

8 Acknowledgments

The first author is grateful to China Scholarship Council (CSC) for the financial support received. The authors also acknowledge the ongoing research collaboration with the University of Liverpool and for their continuous feedback.

References

[1] Da Ronch, A., Badcock, K. J., Wang, Y., Wynn, A., and Palacios, R. N., "Nonlinear Model Reduction for Flexible Aircraft Control Design," *AIAA Atmospheric Flight Mechanics Conference*, AIAA Paper 2012–4404, Minneapolis, MN, 13–16 August 2012, doi: 10.2514/6.2012-4404.

[2] Karpel, M., "Design for Active Flutter Suppression and Gust Alleviation Using State–Space Aeroelastic Modeling," *Journal of Aircraft*, Vol. 19, No. 3, 1982, pp. 221–227, doi: 10.2514/3.57379.

[3] Block, J. J. and Strganac, T. W., "Applied Active Control for a Nonlinear Aeroelastic Structure," *Journal of Guidance, Control, and Dynamics*, Vol. 21, No. 6, 1998, pp. 838–845, doi: 10.2514/2.4346.

[4] Vipperman, J. S., Clark, R. L., Conner, M., and Dowell, E. H., "Experimental Active Control of a Typical Section Using a Trailing–Edge Flap," *Journal of Aircraft*, Vol. 35, No. 2, 1998, pp. 224–229, doi: 10.2514/2.2312.

[5] Da Ronch, A., Tantaroudas, N. D., and Badcock, K. J., "Reduction of Nonlinear Models for Control Applications," *54th AIAA/ASME/ASCE/AHS/ASC Structures, Structural Dynamics, and Materials Conference*, AIAA Paper 2013–1491, Boston, MA, 08–11 April 2013, doi: 10.2514/6.2013-1491.

[6] Schmitt, D., Rehm, W., Pistner, T., Diehl, H., Navé, P., Jenaro-Rabadan, G., Mirand, P., and Reymond, M., "Flight Test of the AWIATOR Airborne LIDAR Turbulence Sensor," *14th Coherent Laser Radar Conference*, Hunstvile, AL, June 2007.

[7] Zeng, J., Moulin, B., De Callafon, R., and Brenner, M., "Adaptive Feedforward Control for Gust Load Alleviation," *Journal of Guidance, Control, and Dynamics*, Vol. 33, No. 3, 2010, pp. 862–872, doi: 10.2514/1.46091.

[8] Da Ronch, A., Tantaroudas, N., and Jiffri, S.and Mottershead, J., "A Nonlinear Controller for Flutter Suppression: from Simulation to Wind Tunnel Testing," *55th AIAA/ASMe/ASCE/AHS/SC Structures, Structural Dynamics, and Materials Conference*, AIAA SciTech 2014, National Harbor, MD, 11–15 January 2014, doi: 10.2514/6.2014-0345.

[9] Ninness, F. and Gustafsson, F., "A Unifying Construction of Orthonormal Bases for System Identification," *IEEE TRANSACTIONS ON AUTOMATIC CONTROL*, Vol. 42, No. 4, 1997, pp. 515–521, doi: 10.1109/9.566661.

[10] Haykin, S., *Adaptive Filter Theory*, chap. 13, Prentice Hall Information and System Science series, 3rd ed., 2001, pp. 566–569.

[11] Papatheou, E., Tantaroudas, N. D., Da Ronch, A., Cooper, J. E., and Mottershead, J. E., "Active control for flutter suppression: an experimental investigation," *International Forum on Aeroelasticity and Structural Dynamics (IFASD)*, Bristol, U.K., 24–27 June 2013.

[12] Fichera, S., Jiffri, S., Wei, X., Da Ronch, A., Tantaroudas, N. D., and Mottershead, J. E., "Experimental and numerical study of nonlinear dynamic behaviour of an aerofoil," *ISMA 2014 Conference*, Leuven, BE, 15–19 September 2014.

9 Contact Author Email Address

Wang, Y.: apple_jw@126.com
Da Ronch, A.: A.Da-Ronch@soton.ac.uk
Ghandchi–Tehrani, M.: M.Ghandchi-Tehrani @soton.ac.uk
Li, F.: caaalifeng@163.com

10 Copyright Statement